ELSEVIER

Journal of Photochemistry and Photobiology A: Chemistry 145 (2001) 183–194

Journal of Photochemistry and Photobiology A:Chemistry

www.elsevier.com/locate/jphotochem

Ultrafast microscopy of laser ablation of refractory materials: ultra low threshold stress-induced ablation

Serguei G. Koulikov[1], Dana D. Dlott*

School of Chemical Sciences, University of Illinois at Urbana-Champaign, Box 01-6 CLSL, 600 S. Mathews Avenue, Urbana, IL 61801, USA

Received 1 April 2001; received in revised form 7 May 2001; accepted 20 June 2001

Abstract

The fundamental mechanisms of photothermal laser ablation of thin films of refractory materials on glass are investigated, using time-resolved microscopy with variable duration ablation pulses (1 ns–10 μs). A fundamental understanding of ablation mechanisms can be used to develop designer materials with ultra efficient ablation, i.e. materials that can be ablated using economical low power laser sources. Refractory Ti and TiN thin film coatings on glass substrates were studied, with the intent of finding materials that can store and then suddenly release a great deal of thermoelastic stress energy that is produced by heating with relatively low intensity laser pulses. Threshold fluences as low as $J_{th} \approx 50\,mJ/cm^2$ were realized. Time-resolved microscopy shows that brittle TiN coatings ablate by violent cracking on all time scales. Similar behavior is observed for Ti, at 1 ns and 110 ns, but at 10 μs the Ti melts but does not ablate. A thermal conduction model is used to show that the temperatures in the coatings at ablation threshold are a factor of 2 (Ti) or 3 (TiN) below the melting point. Calculations of the thermoelastic stress in the coatings shows that stress-assisted ablation occurs when the stored stress energy exceeds the coating adhesion to the substrate by about one order of magnitude. The photothermal stress energy in the coating can be converted almost completely into kinetic energy of the ablated material.

Keywords: Laser ablation; Titanium nitride; Ultrafast microscopy

1. Introduction

In this work, we investigate the fundamental mechanisms of laser ablation of surface layers, using ultrafast time-resolved microscopy [1–5] with ablation pulse durations varied over a wide range 10^{-9}–10^{-5} s [6]. Our intent is to discover mechanisms that can be exploited to obtain surface layer removal at minimal laser fluences or intensities, a process that may be termed "ultra efficient ablation". We have specifically focused on ablation of model systems consisting of a glass substrate and a surface layer of a refractory Ti metal or TiN ceramic thin film. Ablation is a violent irreversible process, and a variety of mechanisms have been proposed depending on the wavelength, pulse duration, fluence and material.[2] Despite these complications, thermodynamics provides a method for finding a theoretical minimum for the ablation fluence threshold J_{th}. The theoretical minimum is equal to the energy of adhesion E_{adh}, which is the amount of work *done on the system* (i.e. $E_{adh} > 0$) to *reversibly* remove the surface layer from the substrate, for instance by slowly peeling it away from the substrate. In real ablation applications, surface layer removal is an *irreversible* process. For this reason, the actual J_{th} must exceed E_{adh} by an amount that depends on the entropy increase associated with irreversible surface layer removal. Understanding the irreversible surface layer removal process and learning how to achieve ablation as close as possible to the theoretical minimum are difficult problems that require investigations of detailed ablation mechanisms.

Many applications, such as pulsed laser deposition, require total vaporization of a surface layer (see Footnote 2). The theoretical minimum J_{th} in that case is that which delivers the enthalpy of vaporization ΔH_{vap} to the surface layer. Typical vaporization fluences for refractory materials or polymers are quite high, often $1–10\,J/cm^2$ for nanosecond pulses (see Footnote 2), and even higher for longer duration pulses. For example, J_{th} increases as $t^{1/2}$ in ablation processes where one-dimensional thermal conduction plays a dominant role [6,8].

Many ablation applications can be engineered to require only that the surface layer or coating be removed from the underlying substrate without regard to whether the coating

* Corresponding author. Tel.: +1-217-333-3574; fax: +1-217-244-3186.
E-mail address: dlott@scs.uiuc.edu (D.D. Dlott).

[1] Present address: Informed Diagnostics, Inc., 1050 E. Duane Avenue, Suite 1. Sunnyvale, CA 94806, USA.

[2] A recent overview can be found in [7].

1010-6030/01/$ – see front matter
PII: S1010-6030(01)00581-0

is vaporized. In that case, the threshold fluence might theoretically be as low as E_{adh}. Even for very durable coatings, E_{adh} will be in the order of only 10–100 μJ/cm^2, suggesting that ultra efficient ablation might be achieved at laser fluences 10 000 or more times lower than the typical 1–10 J/cm^2 mentioned above.

Ultra efficient ablation could have many practical applications in metal, polymer and ceramic layer removal for circuit patterning, mask manufacturing, optical memories, computer-to-press imaging, etc. [9]. Whether an application is economically feasible is determined largely by the cost of the ablation laser source. The number of applications that become economically practical increase rapidly as the cost of the ablation laser decreases. A major break in the cost–benefit curve occurs if the application can be accomplished with an inexpensive compact solid-state source such as a diode laser, rather than the much more costly diode-pumped solid state or excimer lasers [9]. However, diode lasers do not deliver the high power pulses usually associated with ablation. A typical 1 W diode focused to 30 μm diameter produces an intensity of only ∼10^5 W/cm^2. In a few nanoseconds, such a laser can deliver fluences of only a few mJ/cm^2. Higher fluences can be delivered, e.g. 10 J/cm^2 in 100 μs, but such longer pulse durations (dwell times) are often problematic, from the standpoint of J_{th} increasing with dwell time and with the slow work piece flow associated with long dwell times. Ultra efficient ablation would solve these problems: to deliver the hypothetical ∼10 μJ/cm^2 needed to overcome adhesion requires a 1 W diode laser dwell time of only 0.1 ns.

Laser removal of thin substrate-bonded coatings is known to occur by a variety of mechanisms (see Footnote 2). The simplest and most well-understood involves a first-order phase transition, either melting or boiling, of a crystalline material [10,11]. Melting is associated with longer-duration low power pulses. When the coating is heated slowly to the melting point, the surface tension of the melted material causes it to recede away from the center of the heated spot [12,13]. Boiling or superheating is associated with more intense pulses that heat the coating faster than the rate of melt zone retraction [12,13]. High molecular weight organic polymers do not have sharply defined melting or boiling points; instead they evidence a variety of rather gradual softening and flowing transitions, so polymer ablation is never so simple and is not usually associated with melting [14]. However, polymers can be vaporized thermochemically or photochemically, so polymer ablation is usually associated with converting some or all of the polymer layer to a rapidly expanding vapor [4].

In a variety of applications, ablation thresholds that have been observed sometimes were far lower than needed to melt, boil or decompose the coating [15]. These situations are extremely interesting in that they provide insights into mechanisms that can be exploited to reduce ablation thresholds. For instance, several highly efficient surface coating layer removal processes have been discovered recently, where the fluence for nanosecond pulses was quite low [9,16], $J_{th} \sim 20$ mJ/cm^2. These processes involved materials engineered to absorb laser energy only at a very thin (∼30 nm) interfacial layer between the substrate and the surface coating layer. In this case, the threshold fluence could be just enough to vaporize a ∼30 nm thick interfacial layer, destroying the coating–substrate adhesion. The idea of surface coating layer removal by vaporizing only a very thin surface layer was further exploited to reduce J_{th} by an additional factor of 3 at certain pulse durations, by doping the thin interfacial layer with a chemical amplifier — a readily decomposable or energetic polymer such as nitrocellulose [17].

Another interesting mechanism for lower thresholds is termed shock-wave assisted ablation [18], shown schematically in Fig. 1(a) and (b). Shock-wave assisted ablation comes into play when the laser pulse heats a material isochorically — faster than thermal expansion can occur. Since thermal expansion occurs at a typical rate of a few μm/ns, shock-assisted ablation is generally (but not always [12,13,15]) associated with costly high-power sub-nanosecond (ultrashort pulse) lasers. In Fig. 1, a disk-shaped region of a coating on a substrate is isochorically heated (from an initial temperature $T = 0$) to high temperature T. Because the disk is axially confined along the z-axis (it is confined by the substrate on one side and it is inertially confined at the air interface), stress energy $U_c(T)$ builds up inside the disk. The characteristic time for stress energy storage is the inertial confinement time [18]. The disk subsequently undergoes rapid expansion along the z-axis. If the stress energy $U_c(T) > E_{adh}$, this rapid expansion can propel the disk off the substrate, in the z-direction, with a kinetic energy $K \approx U_c - E_{adh}$. Quite large stress energies can be produced. For example, $(\partial P/\partial T)_V \approx 10$ bar/K for the organic polymer poly-methyl methacrylate (PMMA) [18], so a few 100 degree temperature jump can result in stored stress energies in the order of a few $\times 10^9$ J/m^3, or alternatively a few GPa (1 GPa ≈ 10 kbar). In photothermal ablation experiments where PMMA was doped with a near-infrared (near-IR) absorber, Hare et al. [18] found that at ablation threshold $J_{th} = 250$ mJ/cm^2, isochoric heating with 0.1 ns pulses to 280°C generated a stress energy of ∼0.3 GPa, while PMMA thermal decomposition generated ∼0.2 GPa of pressure. Thus at threshold, more of the driving force for ablation could be attributed to stress energy than to polymer vaporization.

In the present work, we investigate whether it might be possible to use processes similar to shock-assisted ablation, that might operate on the longer time scales associated with lower power diode laser ablation, to produce ultra efficient ablation. This requires the ability to store stress energy for times much longer than the sub-nanosecond storage times associated with inertial confinement. Consequently, we have focused on high melting point refractory coating materials such as Ti and TiN. A high melting point means a high temperature and therefore a high stress can be produced before the material loses strength by melting. Additionally,

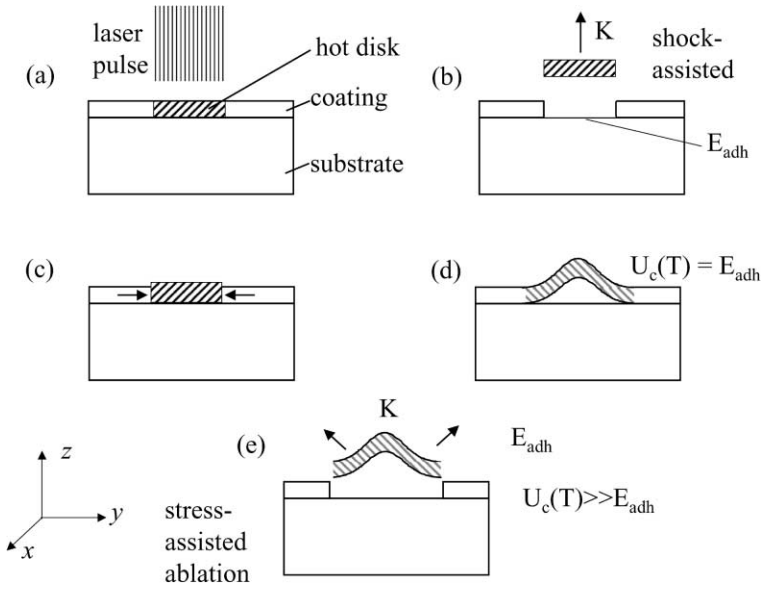

Fig. 1. Shock- and stress-assisted ablation: (a) a laser pulse uniformly heats a thin disk of a coating bonded to a substrate, to a high temperature T; (b) shock-assisted ablation can occur when the pulse duration is shorter than the time for thermal expansion along the z-axis, provided the thermoelastic energy $U_c(T)$ is greater than the effective adhesion energy E_{adh}. The energy difference $U_c(T) - E_{adh}$ appears mainly as kinetic energy K; (c) heating with longer duration pulses coupled with confinement along the x- and y-axis can lead to thermoelastic stress storage for much longer times; (d) the theoretical minimum threshold for removing the coating disk from the substrate occurs when $U_c(T) = E_{adh}$; (e) ablation is a fast irreversible process that occurs only when $U_c(T) \gg E_{adh}$. The excess energy appears mainly as kinetic energy of the coating disk.

a hard or refractory material is capable of storing a great deal of stress for a long time.

The idea behind stress-assisted ablation is shown schematically in Fig. 1(c)–(e). A thin film coating is irradiated with a near-IR laser pulse. Interband transitions in the thin film are excited by the laser. Fast radiationless relaxation leads (typically within a few picoseconds) to the production of heat in the coating. Even though the laser pulse experiences exponential attenuation as it propagates through the coating (in the axial direction), the heat distribution in the axial direction is roughly uniform because thermal conduction is fast over the tens of nanometer length scale of the coating thickness. For pulses with a nonuniform transverse profile (here a Gaussian radial profile), the heat distribution in the coating is nonuniform on the tens of micron scale in the radial direction.

The coating is heated slowly enough to have time for thermal expansion in the axial z-direction. However, the coating is confined in the radial (x and y) directions by the surrounding coating that is not heated by the laser, leading to a build up (Fig. 1(c)) of stress energy $U_c(T)$ that opposes the radial thermal expansion. The minimum *reversible* work for removing a *disk of coating* from a substrate (Fig. 1(d)) is $W_{rev} = E_{adh} + E_{coh}$, where E_{coh} is the cohesive energy between the disk perimeter and the surrounding coating. Ordinarily there is some degree of intrinsic strain U_{c0} in a coating, which depends on details of the growth or deposition process. For a strained coating with adhesive energy E_{adh}, $E_{adh} = E'_{adh} - U_{c0}$, where E'_{adh} is the intrinsic energy of adhesion of a perfect unstrained coating. It is known that U_{c0} can be as much as several GPa, for example, in TiN coatings deposited on rigid noncompliant substrates such as tool steel [19]. However, for a stable coating, U_{c0} cannot exceed E'_{adh}. Experiments that measure the adhesion of a coating for a substrate are actually measuring an effective adhesive energy $E_{adh} = E'_{adh} - U_{c0}$. For large unstrained disks, cohesive effects at the disk perimeter can be neglected so that $W_{rev} \approx E_{adh}$, where E_{adh} is the effective adhesive energy.

Due to the confining effects of the substrate, a sudden release of this stress energy (say by abrupt formation of cracks) will cause the coating to ablate (Fig. 1(e)). This ablation process is fast and *irreversible*. The ablation threshold depends on the detailed dynamics of how the coating is ripped away from the substrate and hurled into space. For this reason, it is difficult to compute the threshold from first principles. The energy balance equation for stress-induced ablation can be written as

$$U_c(T) = E_{adh} + K + Q, \quad (1)$$

where K is the kinetic energy of the ablated coating and Q the heat created by the sudden release of stored stress energy during ablation. For incompressible materials such as Ti and TiN at pressures up to a few GPa, Q is not very large [20], so Eq. (1) shows that the excess thermoelastic stress energy appears mainly as kinetic energy K of the coating (Fig. 1(e)).

If stress-induced ablation can be engineered to become the dominant mechanism of ablation, the actual ablation thresholds for Ti and TiN will depend on well known material parameters such as the bulk modulus, the coefficient of thermal expansion, the thermal conductivity, etc. In

addition, the threshold and the pulse duration dependence of the threshold will depend on properties that are not well known, specifically the detailed nature of the irreversible coating detachment process, and the ability of the coating to store and suddenly release stress energy under conditions of rapid laser heating. In the remainder of this paper, we show how pulse-width dependent ablation threshold measurements and ultrafast microscopy can be used to study these processes, and how long-term storage of stress energy can be used to produce low ablation thresholds even with long duration, low power laser pulses.

2. Experimental

Titanium ($T_{m.p.} = 1675°C$) and titanium nitride ($T_{m.p.} = 2930°C$) [21] coatings sputtered onto low thermal expansion glass substrates were provided by Thomas E. Lewis and Ernest W. Ellis of Presstek (Nashua, NH). The coatings were optimized for maximum absorption in the near-IR, and minimum ablation thresholds, which led to a coating thickness of ~60 nm. The intrinsic coating stress and the coating adhesion were individually unknown. However, by observing intrinsic blister defects in a Ti coatings, as described in Section 3.1, we were able to estimate an upper limit to the Ti on glass adhesion energy E_{adh} to be 15 μJ/cm^2.

The coatings were ablated by Gaussian spatial profile near-IR 1064 nm pulses from Nd solid-state lasers. The ablation pulses were incident on the coating surface (Fig. 1(a)). Three pulse duration (t_p) were used: 1 ns, 110 ns, and 10 μs. The 10 μs pulses were produced by chopping the output of a continuous laser (Quantronix 116) with an acousto-optic modulator. The 110 ns pulses were produced by Q-switching the same laser. The 1 ns pulses were generated by a Q-switched microlaser (Newport, model NP-1030-10). The beam diameter ($2w$ at the $1/e^2$ intensity points) of the focused laser beams at the sample surface was 48 μm. A Si photodiode calibrated against a laser power meter (Coherent) was used to measure laser pulse energy E_p.

The ultrafast microscopy apparatus [9] is diagrammed in Fig. 2. The microscope (Olympus, BX60M) could be illuminated by a tungsten lamp or a sub-nanosecond laser pulse. The image was captured with a CCD camera (Sony, SSS-M254), a personal computer, a video frame grabber and image analysis software (Data Translation Global Lab Image^{TM}).

For threshold measurements, the sample was placed on the microscope stage with the coating facing up. The coatings were ablated and imaged in situ. A pellicle dichroic beam-splitter (National Photocolor, Mamaroneck, NY) was placed at 45 degrees between the objective and the sample to reflect the near-IR pulse onto the sample surface while allowing the sample to be viewed with visible illumination. Images obtained with the CCD camera and frame grabber were analyzed by image analysis software (Data Translation Global Lab Image^{TM}) to determine the ablated area.

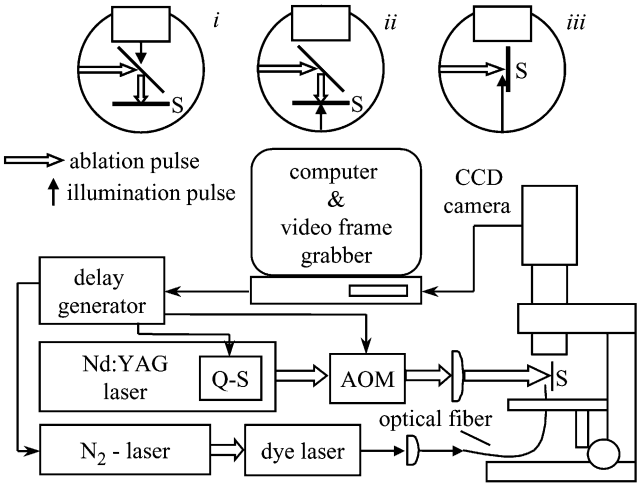

Fig. 2. Schematic of fast microscopy apparatus. Key: QS, acousto-optic Q-switch; AOM, acousto-optic modulator; S, thin film sample. (i), (ii) and (iii). Arrangements for time-resolved imaging of ablation in reflection, transmission and grazing incidence, respectively. In (i) and (ii) the ablation pulse is reflected from a pellicle beamsplitter that transmits the visible observation pulse.

For time-resolved microscopy, the illumination source was a sub-nanosecond visible pulse from a home built dye laser (Coumarin 500 dye) pumped by a high-pressure nitrogen laser (Laser Photonics, LN203C). The frame grabber, near-IR laser and illumination laser were triggered by a home built pulse delay generator [22]. The samples were observed with three different geometries [2] shown in Fig. 2. For reflection and transmission measurements, the pellicle was used. Images acquired at a variety of delay times were reconstructed to give a stroboscopic "movie" of ablation. These are only true movies to the extent that each single-shot event is identical [22]. The samples are highly uniform and the lasers are stable, so the ablation process is reproducible overall, but each shot differs in detail. Cracks or droplets are not identical from frame to frame. Images at a given delay were obtained in sets of three, and the reconstructed movies were produced by selecting one image of three that was deemed representative.

3. Results

3.1. Adhesion energy

The adhesion energy E_{adh} was estimated by observing blister defects in the coatings [23], such as the representative image shown in Fig. 3. This image shows a nearly hemispherical blister in Ti coated on glass. This blister was formed during the coating process, when the local stress energy exceeds the energy of adhesion, so we assume it forms gradually enough to represent a nearly reversible coating removal process. From the reflected light image at left, we can determine the radius r. The fringes (Hg lamp, 565 nm)

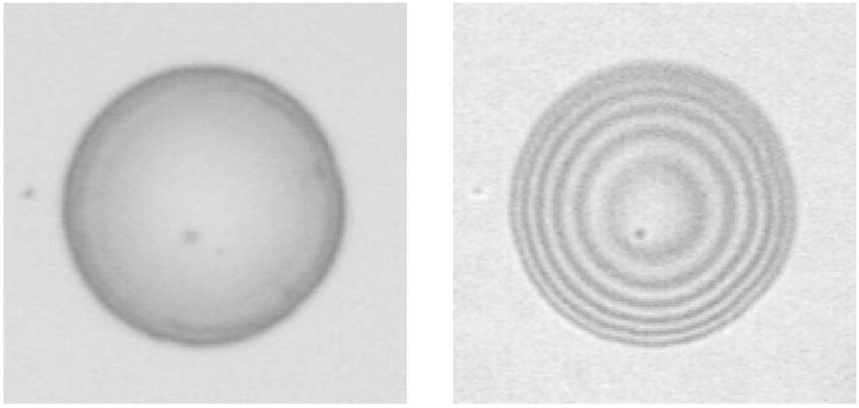

Fig. 3. A blister defect in the Ti coating on glass in reflection (left) and transmission (right). From the defect diameter and the blister height measured by counting the interference fringes, the effective adhesion E_{adh} (the intrinsic adhesion E'_{adh} minus the intrinsic coating strain U_{c0}) is determined to be $E_{adh} \approx 15\,\mu J/cm^2$.

in the transmitted light image at right give the blister height h. The surface area S is $S \approx \pi(h^2 + r^2)$, while the area of the base is $S_0 = \pi r^2$, so

$$\frac{S - S_0}{S_0} = \left(\frac{h}{r}\right)^2. \tag{2}$$

The stress in the coating that led to the formation of this defect, σ_{c0}, is equal to the stress needed to compress the coating area from S back to S_0

$$\sigma_{c0} = \frac{E_c}{2(1-\nu_c)}\left(\frac{h}{r}\right)^2, \tag{3}$$

where E_c is the Young's modulus and ν_c the Poisson ratio [23]. Averaging over several defects seen in the coating, we found that the stress energy $U_{c0} = 15 \pm 2\,\mu J/cm^2$, where

$$U_{c0} = \sigma_0^2 \frac{1-\nu_c}{E_c} d_c, \tag{4}$$

and d_c is the coating thickness. Blister defects are formed only in regions where $U_0 \geq E'_{adh}$, [23] so $E_{adh} = E'_{adh} - U_{c0} \approx 15\,\mu J/cm^2$. As described in the introduction, the effective adhesion energy E_{adh} provides a reasonable estimate for W_{rev}, the minimum work needed to remove the coating from the substrate.

3.2. Ablation threshold measurements

For a Gaussian radial intensity profile, the fluence $J(r)$ for a pulse with energy E_p is a radial function of the distance r from the beam center

$$J(r) = \frac{2E_p}{\pi w^2} \exp\left(-\frac{2r^2}{w^2}\right), \tag{5}$$

where w is the Gaussian beam radius. For a material with a sharp ablation threshold fluence J_{th} (J_{th} is usually an increasing function of pulse duration), the ablated area S is given by [24,25]

$$S = 0, \quad J(0) \leq J_{th}, \tag{6a}$$

$$S = \frac{\pi w^2}{2} \ln\left(\frac{2E_p}{J_{th}\pi w^2}\right), \quad J(0) > J_{th}, \tag{6b}$$

where $J(0) = 2E_p/\pi w^2$ is the fluence at the center of the beam. Eq. (6b) shows the ablated area S increases with increasing fluence above J_{th}, and that a plot of S versus $\ln(E_p)$ should be linear [17]. (A nonlinear plot indicates that J_{th} changes with intensity, presumably due to the presence of more than one competing ablation mechanism [17].) The slope of the line is proportional to w, and the line crosses the abscissa at $E_p = 2J_{th}\pi w^2$. Threshold data at three pulse durations for Ti and TiN are shown in Figs. 4 and 5. Thresholds obtained from these data are listed in Table 1. The

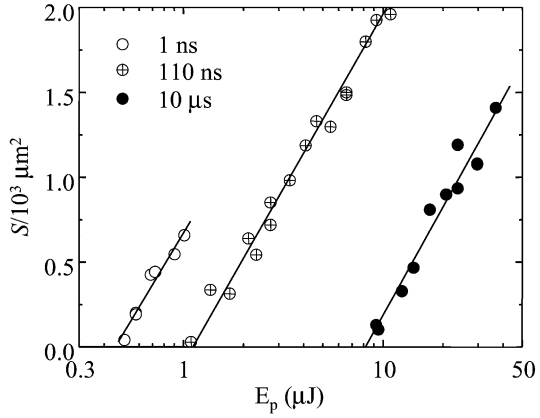

Fig. 4. Ablation thresholds of Ti on glass. Plots of the area S of the ablated spot versus the logarithm of the pulse energy E_p for 1 ns, 110 ns and 10 μs pulses. The slope gives the Gaussian beam radius w. The x-intercept gives the threshold pulse energy E_p. Knowing E_p and w, the threshold fluence J_{th} is determined. The values of J_{th} are given in Table 1.

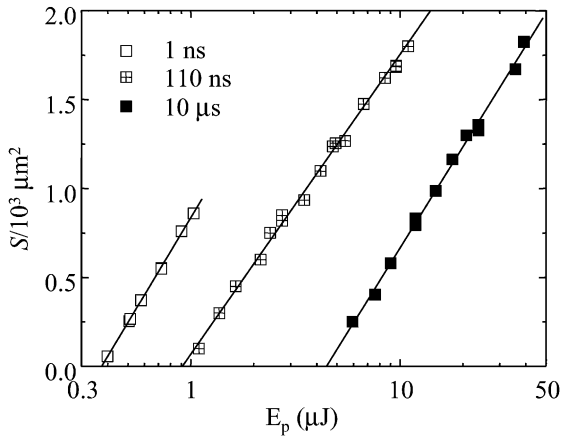

Fig. 5. Ablation thresholds for TiN on glass. Plots of the area S of the ablated spot versus the logarithm of the pulse energy E_p for 1 ns, 110 ns and 10 μs pulses. The values of J_{th} are given in Table 1.

Table 1
Single-shot ablation thresholds for 60 nm Ti and TiN on glass for pulse duration t_p

Coating	$t_p = 1$ ns	$t_p = 110$ ns	$t_p = 10$ μs
Ti	53 ± 3 (mJ/cm^2)	127 ± 4 (mJ/cm^2)	888 ± 32 (mJ/cm^2)
TiN	43 ± 1 (mJ/cm^2)	111 ± 4 (mJ/cm^2)	557 ± 9 (mJ/cm^2)

error bars ($\pm 1\sigma$) are obtained using standard linear regression analysis methods.

From a known threshold, it is possible to determine the "point of maximum efficiency" for a Gaussian profile pulse. A Gaussian profile simultaneously irradiates a sample with a range of fluences. At the point of maximum efficiency for a material with threshold J_{th}, the ratio of the ablation spot area S to the pulse energy E_p is a maximum [26]. This point occurs when a pulse of Gaussian beam radius w (which denotes the $1/e^2$ intensity point) produces a spot of area $S = \frac{1}{2}\pi w^2$. The fluence at the beam center is then $\exp(1) J_{th} \approx 2.7 J_{th}$. Because J_{th} varies a great deal with pulse duration, in order to facilitate comparisons between measurements at different pulse durations, all microscopy data described below were obtained by adjusting the intensity at each pulse duration to be close to this point of maximum efficiency. In that case, each pulse duration produced an ablation spot of approximately the same area.

3.3. Absorption, transmission and reflectivity

For subsequent thermal calculations, we need to know how much 1064 nm energy is absorbed by the coating. The absorption coefficient k_a is obtained using $k_a = 1 - k_r - k_t$, where k_r is the reflection coefficient and k_t the transmission coefficient [8]. The values of k_r and k_t were measured in two different ways. First, we measured the reflected and transmitted intensities of a weak continuous 1064 nm laser beam, giving the reflectivity and transmittance of the sample near room temperature. The transmission measurements needed to account for reflections at the substrate–air interface, which were measured using a substrate with the coating fully ablated away. The results are given in Table 2. To check for the possibility that the absorption might change significantly during ablation, we used a 1 ns laser pulse at a fluence corresponding to the point of maximum efficiency. With a 1 ns pulse, there is not enough time for the motion of the ablated coating material to scatter the transmitted light. The 1 ns results are also given in Table 2. The absorption measurements using the two methods are within 4% of each other, so we conclude that the coating optical properties do not change significantly (±4%) during laser heating towards ablation. This conclusion agrees with earlier work with Al thin film coatings [8].

3.4. Time-resolved microscopy

Stroboscopic images of Ti and TiN ablation using 1 ns, 110 ns and 10 μs pulses at the point of maximum efficiency are shown in Figs. 6–9. The reflection images observe the coating surface. The transmission images indicate when and where the coating has ablated. Because the coating transmission is just a few percent, when the coating is ablated the transmission increases abruptly and a bright spot is observed. The grazing incidence images show material ejected from the substrate surface [2].

Ablation with 1 ns pulses in both Ti and TiN (Fig. 6) results in a solid disk of material being forcefully expelled from the substrate. With both coatings, but most clearly with the Ti coating, transmission images show interference fringes at short times that result from a gap developing between the coating and the substrate. Appearance of the fringes indicates the approximate instant when the coating breaks away from the substrate. At this instant, significant thermal conduction to the substrate ceases and subsequent laser pulse heating becomes adiabatic. The expelled disks

Table 2
Reflection coefficient k_r, transmission coefficient k_t, and absorption coefficient k_a for Ti and TiN on glass with 1064 nm low intensity light and with 1 ns ablation pulses

Coating	k_r	k_t	k_a	k_r (1 ns)	k_t (1 ns)	k_a (1 ns)
Ti	0.60 ± 0.02	0.049 ± 0.005	0.35 ± 0.03	0.61 ± 0.03	0.05 ± 0.01	0.34 ± 0.04
TiN	0.49 ± 0.02	0.083 ± 0.005	0.42 ± 0.03	0.47 ± 0.02	0.08 ± 0.01	0.44 ± 0.03

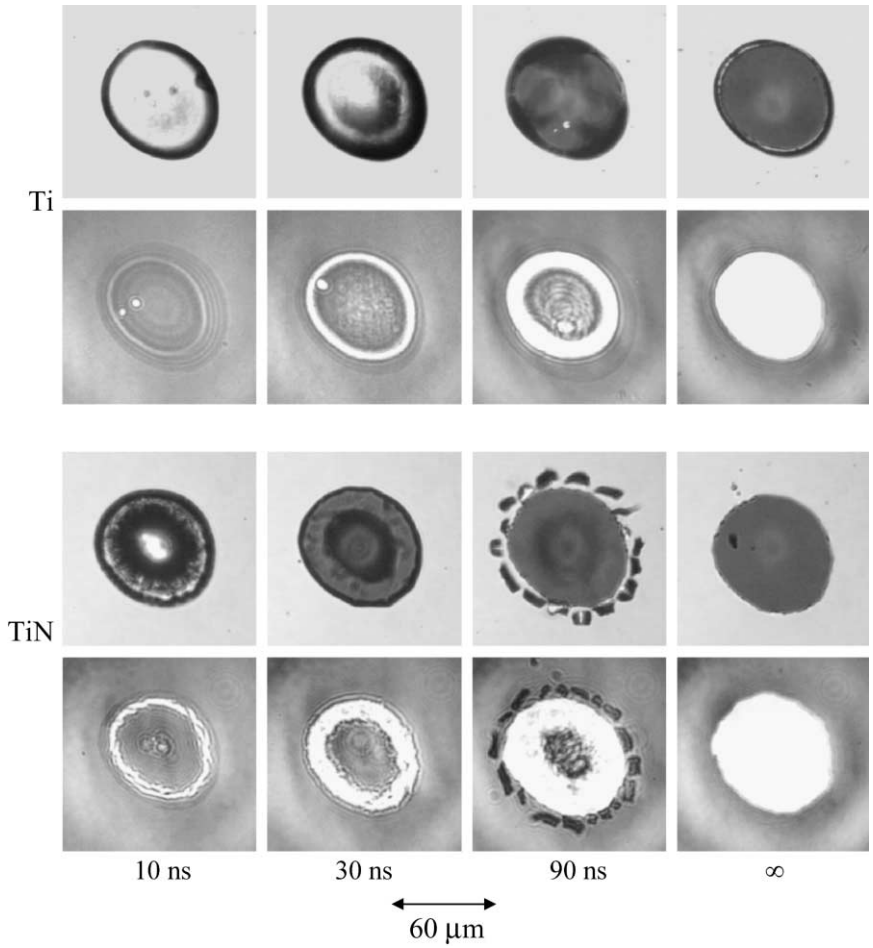

Fig. 6. Time-resolved micrographs of 1 ns pulse ablation of Ti (top two rows) and TiN (bottom two rows) at indicated times. The image size is 60 μm × 60 μm. The top rows are obtained in reflection and the bottom rows are obtained in transmission. The ablated spot diameter is ∼50 μm. At short times, interference fringes are seen that indicate the coating has lifted off the substrate. The coating is ablated as a nearly intact disk. At longer times, the TiN coating undergoes fragmentation.

are heated nonuniformly by the Gaussian beam, which is ≈2.7 times more intense at the disk center than at the disk edge. This nonuniform heating causes the ductile Ti disk to buckle. Ablation of TiN is similar to Ti ablation except that for times >30 ns the brittle TiN disk begins to disintegrate into a shower of cracked TiN shards.

Ablation with 110 ns pulses is shown in Fig. 7 (Ti) and Fig. 8 (TiN). These figures were originally appeared in [9], where they were presented with little discussion. The coating breaks away from the substrate in the first few tens of ns, as indicated by the interference fringes. The motion of the coating through the air generates a shock wave in the air. This type of shock in air originating from a central source is usually termed a blast wave [1,20]. The bright spots seen in grazing incidence images in the 20–200 ns time range are artifacts due to reflections of the illumination pulse back into the camera from a point on the spherical blast front. Some time after the Ti coating leaves the substrate, it begins to violently expel Ti droplets, which suggests that the Ti at the center of the spot has been superheated past the melting point and is boiling off (Fig. 7). The TiN coating appears never to melt. It first develops a complicated wrinkle pattern. Then once it leaves the substrate, it begins to crack and break apart into TiN flakes that eventually settle back onto the substrate (Fig. 8).

Fundamentally different behavior is observed when 10 μs pulses are used (Fig. 9). As in Figs. 6–8, the first indication of coating removal, the appearance of interference fringes in transmission, occurs at 1.5–2.0 μs. With Ti at 10 μs, the mechanism of coating removal is the familiar melting and receding of liquid Ti away from the center of the heated spot [12,13]. Ultimately, a bead of solidified Ti is left surrounding the perimeter of the spot. With TiN, the heated brittle ceramic bulges up off the surface and then suddenly undergoes violent cracking, which removes the coating and leaves TiN flakes scattered over the substrate. Although the ablated spot in Fig. 9 is highly irregular, if the TiN is gently cleaned with a soft cloth and some rubbing alcohol, a round spot is exposed [17], comparable in sharpness to those observed with shorter pulse durations.

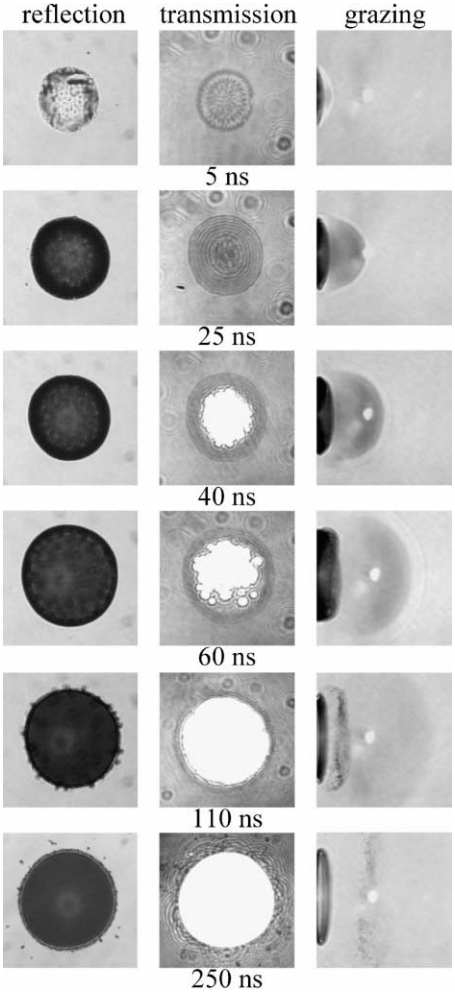

Fig. 7. Images of 110 ns pulse ablation of Ti on glass. The image size is 60 μm × 60 μm. By 5 ns, the coating has begun to lift off the substrate. By 40 ns, the appearance of a bright spot in the transmission images indicates Ti has left the substrate. Ti droplets are seen scattered around the ablated spot. In the grazing incidence images, the dark region is the moving Ti coating. A blast wave in the air is seen at right. The bright spot is an artifact due to a reflection into the camera from the blast wave front. Images reproduced with permission from [9].

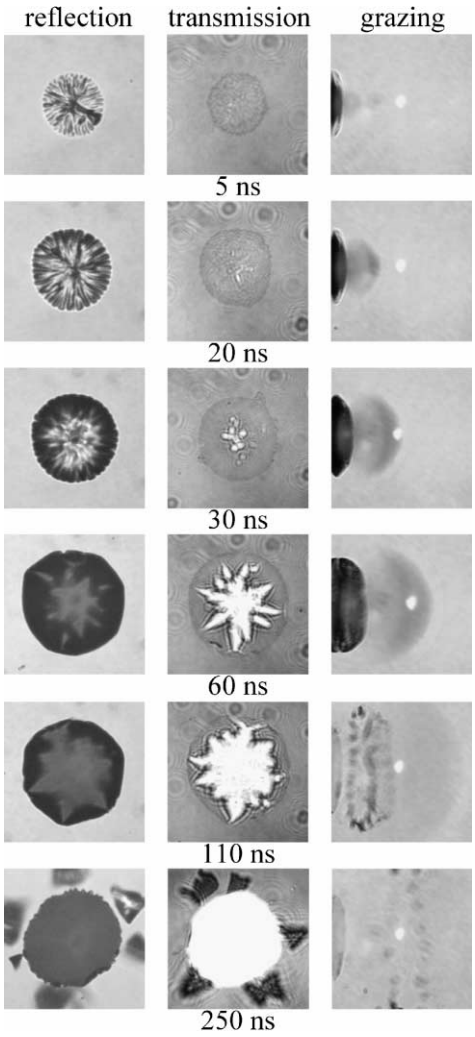

Fig. 8. Images of 110 ns pulse ablation of TiN on glass. The image size is 60 μm × 60 μm. By 5 ns, the coating has begun to buckle and to lift off the substrate. By 30 ns, the TiN coating has begun to fragment. Images reproduced with permission from [9].

3.5. Kinetic energy of ablation

Using grazing incidence images of Ti and TiN samples, the speed and kinetic energy of the ablated coating could be measured [1]. In Fig. 10, the distance between the ablated material and the surface of the sample is shown as a function of time for 1 and 110 ns ablation. Time zero was the time the coatings started to separate from the substrate. Keep in mind that the fluence at 1 ns is about three times lower than at 110 ns (see the measured thresholds in Table 1). The initial velocities of the ablated materials are about the same for both pulse durations and the coating decelerates after a while, presumably due to air resistance. The initial velocities are $V \approx 110\,\mathrm{m/s}$ for TiN and $V \approx 95\,\mathrm{m/s}$ for Ti at both pulse durations. Using the density and thickness of the coating materials from Table 3, the kinetic energy

Table 3
Thermophysical properties of Ti and TiN

Thermophysical properties	Ti	TiN
Density (g/cm^3)	4.54[a]	5.22[a]
Specific heat at 25°C (J/g °C)	0.52[a]	0.60[b]
Thermal conductivity (W/cm °C)	0.22[b]	0.192[b]
$T_{\alpha\rightarrow\beta}$ (°C)	882[a]	
$\Delta H_{\alpha\rightarrow\beta}$ (J/g)	83.0[a]	
T_m (°C)	1675[a]	2930[a]
ΔH_m (J/g)	402[a]	
T_b (°C)	3260[a]	
ΔH_b (J/g)	8828[a]	
Young's modulus (GPa)	116[b]	600[b]
Poisson's ratio	0.32[b]	0.25[b]
Thermal expansion coefficient (°C^{-1})	8.6×10^{-6}[a]	6.3×10^{-6}[a]

[a] [21].
[b] [27].

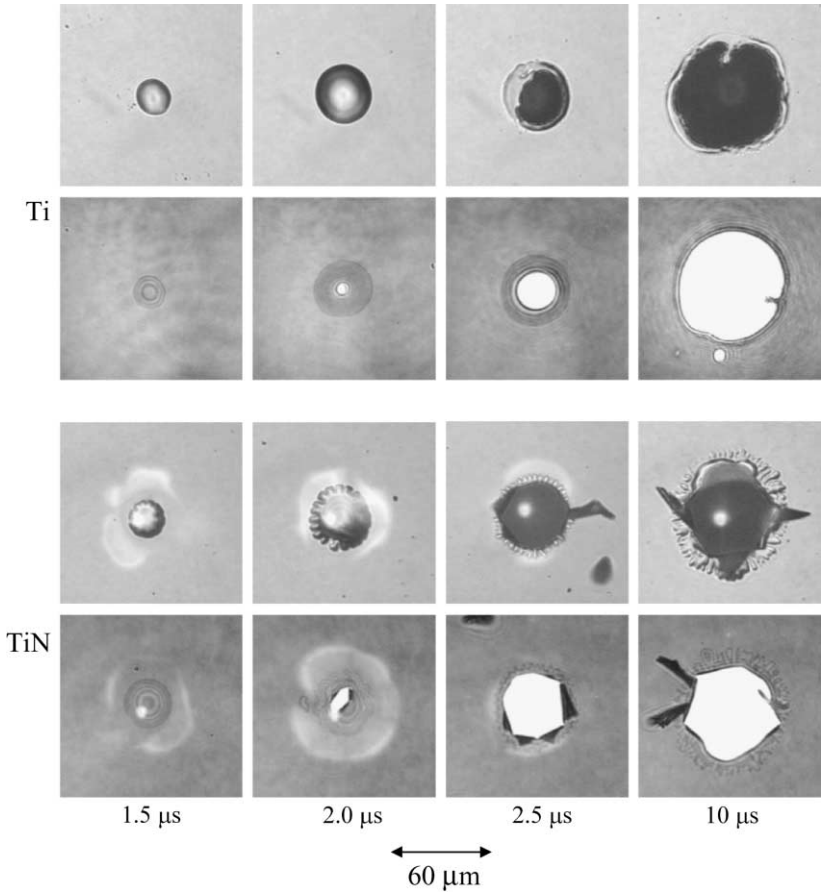

Fig. 9. Images of 10 μs pulse ablation of Ti (top two rows) and TiN (bottom two rows) on glass. The image size is 60 μm × 60 μm. The top rows of each panel are obtained in reflection and the bottom rows are obtained in transmission. The Ti coating melts and recedes away from the laser-heated region. The TiN coating ablates by abrupt fragmentation beginning at about 2.0 μs.

per unit area of ablated material is $K_{Ti} \approx 120\,\mu J/cm^2$ and $K_{TiN} \approx 190\,\mu J/cm^2$. These kinetic energies are much greater than the adhesive energy of Ti on glass, $E_{adh} \approx 15\,\mu J/cm^2$.

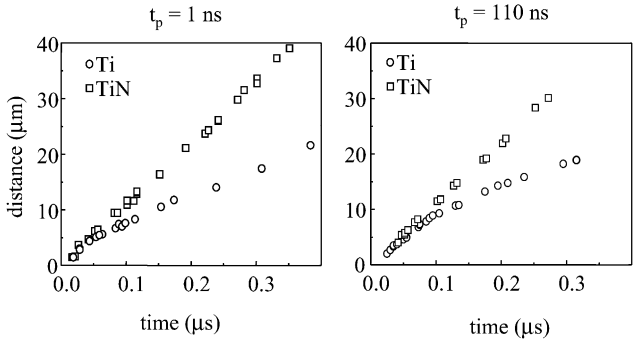

Fig. 10. Plots of the time-dependent location of Ti and TiN ablation debris. The 1 ns fluence is about three times less than the 110 ns fluence, so the ablated spots have about the same diameter. The slopes of the lines at shorter times give the kinetic energy of the ablated coating disks, which are in the range 100–200 $\mu J/cm^2$.

4. Discussion

4.1. Summary of ablation results

Ultrafast imaging of TiN ablation with pulses in the range 1 ns–10 μs show the same mechanism dominates at all times; the TiN coating explodes into jagged shards. Because there appears to be no vaporization or melting, and because the time scales rule out shock-assisted ablation (the inertial confinement time in these 60 nm layers is only ∼15 ps), TiN ablation appears to occur via the stress-assisted ablation mechanism described earlier and in Fig. 1. Consequently, these data indicate that TiN coatings can store thermoelastic stress for durations of at least several microseconds.

With Ti ablation, we see different mechanisms in the range 1 ns–10 μs. With 1 ns pulses, we see a Ti disk ablating almost intact without melting or boiling, similar to what is expected for stress-assisted ablation. Thus, we attribute the 1 ns Ti ablation to stress-assisted ablation. With 110 ns pulses, we see Ti ablating, but we also see the Ti disk expels droplets or chunks that appear to be molten Ti, which suggests that stress-induced ablation is accompanied by Ti boiling. With

10 μs pulses, we see no evidence for stress-assisted ablation, merely Ti melting and a receding melt front.

4.2. Temperature calculations

The temperature in the laser-irradiated coating was calculated with a thermal conduction model described previously [6,8,22]. We assume that thermal conduction is dominated by one-dimensional conduction along the *z*-axis perpendicular to the substrate. This approximation is accurate because the beam diameter is much larger than both the coating thickness and the thermal diffusion length [6]. Even though there is exponential attenuation of the laser pulse in the coating, which in the absence of thermal conduction would lead to a large temperature gradient between the air and the substrate interface, we assume thermal gradients within the coating along the *z*-direction vanish almost immediately because the coating is only 60 nm thick and thermal conduction within the coating is facile [6]. The heat capacities of Ti and TiN are well known in the relevant temperature range [21]. Ti has a solid–solid phase transition ($\alpha \rightarrow \beta$) at 882°C. For simplicity, we used ambient temperature parameters for the glass substrate. Ignoring the temperature dependence of the glass thermal conductivity creates little error. The temperature T of a coating initially at T_0 ($T_0 = 25$°C) can be expressed as a function of the laser fluence J

$$\rho_c d_c \left(\int_{T_0}^{T} \mathrm{d}T'\, C_c(T') + \sum_i \Delta H_i \right) + (T - T_0)\frac{\sqrt{\pi \rho_s C_s \kappa_s t_p}}{2} = k_a J, \quad (7)$$

where $k_a J$ is the fraction of incident fluence that is absorbed, the subscripts c and s refer to coating and substrate, ρ the density, C the specific heat, κ_s the substrate thermal conductivity, d_c the coating thickness and ΔH_i the enthalpy of phase transition(s). The parameters [21,27] used to evaluate Eq. (7) are listed in Table 3.

The first term in Eq. (7) describes adiabatic heating of the coating. It is independent of pulse duration t_p and any substrate parameters. The second term, which is proportional to $(t_p)^{1/2}$ and $(\kappa_s)^{1/2}$, describes heat dissipated into the substrate by thermal conduction. Eq. (7) ignores the possibility of the coating dynamically debonding from the substrate during the laser pulse, which will be discussed in a moment.

Figs. 11 and 12 are calculations of the temperatures of the Ti and TiN coatings on glass, for irradiation by a pulse of the indicated duration with fluence J. The dotted curve ("adiabatic") is due to the first term in Eq. (7) alone, which describes the temperature rise of a coating not thermally contacted to a substrate. As the pulse duration is increased at constant fluence, the temperature increase becomes smaller due to thermal loss from the coating to the substrate.

The ablation threshold fluences J_{th} measured with 1 ns, 110 ns and 10 μs pulses are also indicated in Figs. 11 and 12. The values of the different temperature curves at J_{th} gives the calculated ablation temperature for each pulse duration. The calculated ablation temperatures T_{abl} were approximately independent of pulse duration for a given material. When T_{abl} changes very little with pulse duration t_p over a vast range of durations (here 10^{-9}–10^{-5} s), it is likely that the ablation mechanism is independent of pulse duration and that almost all the increase in J_{th} with increasing t_p is due to the need to overcome thermal loss from the coating to the substrate. The computed ablation temperatures were

$T_{abl} \sim 900$°C (Ti on glass), $T_{abl} \sim 800$°C (Ti on glass).

It is apparent that these calculated threshold temperatures are *far below the melting points*. In fact, the threshold

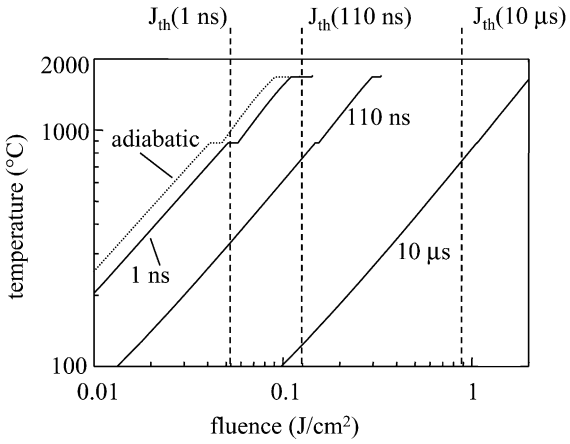

Fig. 11. Calculations of the temperature of the coating disk as a function of pulse fluence for Ti on glass. The adiabatic curve assumes no thermal loss to the substrate. In the actual ablation process, there is a pulse-duration dependent thermal loss to the substrate. When the coating leaves the surface, heating abruptly becomes adiabatic. The measured threshold J_{th} for each pulse duration intersects these heating curves at a point that gives a lower limit for the ablation temperature of ~900°C, a factor of 2 below the melting point.

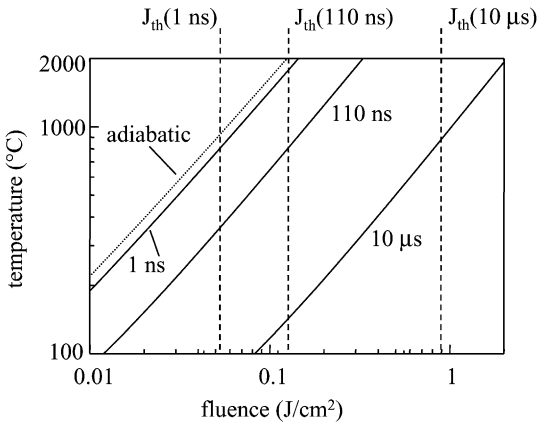

Fig. 12. Calculations of the temperature of the coating disk as a function of pulse fluence for TiN on glass. The measured threshold J_{th} for each pulse duration intersects these heating curves at a point that gives a lower limit for the ablation temperature of ~800°C, a factor of 3 below the melting point.

temperature is lower for TiN ($T_{\mathrm{m.p.}} = 2930^{\circ}\mathrm{C}$) than for Ti ($T_{\mathrm{m.p.}} = 1675^{\circ}\mathrm{C}$), despite the higher melting point of TiN. These low temperatures are further evidence for stress-assisted ablation.

We now return to the problem of dynamic debonding. When the coating debonds from the substrate, thermal conduction ceases. (However, radiative and convective heat losses might still be significant, especially for very small gaps between coating and substrate and for longer duration pulses.) If dynamic debonding occurs during the laser pulse, it leads to a sudden jump in the effective heating rate, and the calculations in the figures will underestimate T_{abl}. However, dynamic debonding is clearly not a factor in the calculations with 1 ns pulses because debonding is first observed after several nanoseconds, well after laser heating ceases. Thus the ablation temperatures listed above are essentially correct for 1 ns pulses. With longer duration pulses, debonding starts to occur part way through the pulse, leading to a somewhat higher coating temperature than suggested by the heating curves in Figs. 11 and 12. Dynamic debonding helps to explain the 10 μs ablation of Ti seen in Fig. 9, where the coating is obviously above the melting point, and the 110 ns ablation of Ti seen in Fig. 8 where the coating appears to boil. Due to uncertainties in computing the temperatures with 110 ns and 10 μs ablation, further quantitative discussions will be limited to the case of 1 ns ablation.

4.3. Thermoelastic stress

Stress-assisted ablation can occur when the stored thermoelastic energy $U_{\mathrm{c}}(T)$ exceeds the adhesion energy E_{adh} by some amount not deducible from first principles, which depends on the detailed dynamics of the fast irreversible destruction of the coating–substrate interfacial region. This excess $U_{\mathrm{c}}(T)$ appears mainly as kinetic energy K, as described in Eq. (1).

The coating has thermal expansion coefficient α_{c}. Stress is produced by the heated coating disk trying to expand against the colder surrounding coating (Fig. 1(c)), and also by any mismatch in thermal expansion between coating and substrate. Our samples are fabricated on low thermal expansion glass, so the thermal expansion coefficient for the substrate $\alpha_{\mathrm{s}} \approx 0$. We begin with the simplified case of a circular disk of radius r_0 heated *uniformly* (say by a laser with a uniform top hat profile) from temperatures T_0 to T, while the surrounding coating is held at T_0. The stress in the coating is the sum of the intrinsic stress σ_{c0} and the temperature-dependent stress $\sigma_{\mathrm{c}}(T)$, where $\sigma_{\mathrm{c}}(T)$ is given by [28]

$$\sigma_{\mathrm{c}}(T) = \alpha_{\mathrm{c}}(T - T_0)\frac{E_{\mathrm{c}}}{1 - \nu_{\mathrm{c}}}. \tag{8}$$

In actual experiments, the coating is heated by a pulse with a Gaussian radial profile. It is straightforward to calculate the radial and tangential stress profile in this case, as described in Section 15.6.12 of [28]. The radial stress profile $\sigma_{\mathrm{c}}(r, T)$ in the absence of radial thermal conduction can be found using Eq. (8) and the radial Gaussian beam profile. In a system with radial thermal conduction, the temperature and stress at the edge of the spot is always a bit greater than predicted on this basis due to thermal conduction from the hotter center to the colder edge. Thus Eq. (8) should be regarded as a lower limit to the thermal stress with Gaussian pulse heating.

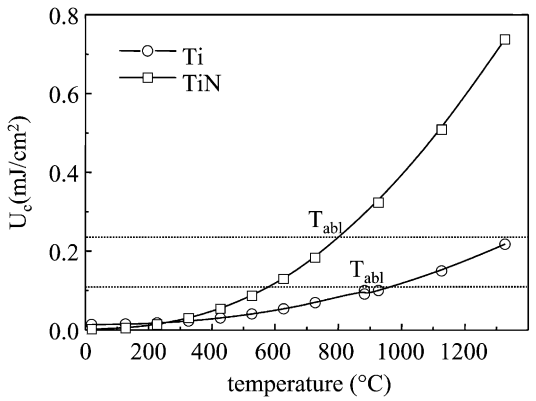

Fig. 13. Computed values, using Eq. (9), of the thermoelastic stress $U_{\mathrm{c}}(T)$ as a function of T for Ti and TiN on glass. The dotted lines cross the $U_{\mathrm{c}}(T)$ curves at the computed ablation temperature T_{abl}. The corresponding thermoelastic stress at ablation threshold for Ti is 100 μJ/cm^2, and for TiN is 230 μJ/cm^2.

The increase in stress energy per unit area in the coating due to heating to temperature T, $U_{\mathrm{c}}(T)$ is

$$U_{\mathrm{c}}(T) = \sigma_{\mathrm{c}}^2(T)\frac{1 - \nu_{\mathrm{c}}}{E_{\mathrm{c}}}d_{\mathrm{c}}. \tag{9}$$

In Fig. 13, the computed stress energies $U_{\mathrm{c}}(T)$ are shown for Ti and TiN. The values of $U_{\mathrm{c}}(T)$ at the ablation temperatures given above are ∼100 μJ/cm^2 for Ti (900°C) and ∼230 μJ/cm^2 for TiN (800°C). The corresponding kinetic energies of ablation were 120 μJ/cm^2 for Ti and 190 μJ/cm^2 for TiN. *The computed thermoelastic stress energy at ablation threshold is quite close to the measured values of the coating kinetic energy K* and *about an order of magnitude greater than the estimated effective coating adhesive energy* $E_{\mathrm{adh}} \approx 15\,\mu\mathrm{J/cm}^2$. The good agreement between computed stress energies and measured ablation kinetic energies reinforces the conclusion that stress-assisted ablation is dominant. In addition, this agreement shows a high efficiency of conversion of stress energy into kinetic energy of ablation.

5. Conclusions

Stress-assisted ablation is observed in TiN coatings and in Ti coatings with shorter duration (1–110 ns) pulses. The thermoelastic calculations indicate highly efficient conversion of stored stress energy into coating kinetic energy. For our Ti and TiN samples, the ablation threshold is quite low, only ∼50 mJ/cm^2 for a 1 ns pulse. To put this in perspective,

the thermal calculations show these thresholds are a factor of 2 or 3 below what is needed to melt the coating, let alone vaporize it. The ablation threshold increases substantially (a factor of 10 in going from 1 ns to 10 μs) for longer duration pulses, but the thermal conduction model reveals that up to 10 μs pulse durations, much of this increase is due to the heat lost to the substrate.

The goal of utilizing stress-assisted ablation to achieve material ablation with a low power laser has been achieved. Given the measured 10 μs threshold of the TiN sample, ablation of a 10 μm diameter region could be achieved with a 40 mW diode laser. If thermal dissipation to the substrate could be successfully overcome, a 4 mW diode would suffice.

In Section 1, we mentioned two crucial unanswered questions regarding stress-induced ablation: (1) how long can stress be stored — the longer the storage time the lower the intensity needed for ablation; (2) by how much does the stored stress need to exceed the adhesive energy for ablation to occur. Now we have some answers to these questions: in TiN, 10 μs stress energy storage times are attainable, and the stored energy needs to exceed the adhesion by about a factor of 10 before the coating can be forcibly ejected from the substrate.

Now that we have realized the concept of using stored stress to lower ablation thresholds, it becomes possible to speculate how materials engineering might be used to make lower threshold ablation materials. For low intensity long duration pulses, thermal loss to the substrate plays a significant role in increasing the threshold. This knowledge suggests a possible strategy for lowering the ablation threshold for longer duration pulses: adding a thermal barrier layer between the coating and substrate. A more sophisticated strategy might involve designing coating materials to enhance the dynamic debonding effect, which can cause a sudden shut off of thermal loss during the laser pulse. Besides a high melting point and high absorption of near-IR light, other properties of an ablatable coating which enhance stress-assisted ablation are a large coefficient of thermal expansion and a large Poisson ratio. Solid–solid phase transitions such as the $\alpha \rightarrow \beta$ transition in Ti might also be exploited to enhance stress-assisted ablation.

Acknowledgements

This work is based on research supported by a grant from Presstek, Inc., and US Army Research Office contract DAAD19-00-1-0036. Partial support from the US Air Force Office of Scientific Research contract F49620-00-1-0049 is also acknowledged.

References

[1] H. Kim, J.C. Postlewaite, T. Zyung, D.D. Dlott, J. Appl. Phys. 64 (1988) 2955.
[2] S.G. Koulikov, D.D. Dlott, in: Advances in Non-impact Printing Technologies, Vol. 14, Society for Imaging Science and Technology, Springfield, VA, 1998, p. 172.
[3] I.-Y.S. Lee, W.A. Tolbert, D.D. Dlott, M.M. Doxtader, D.M. Foley, D.R. Arnold, E.R. Ellis, J. Imag. Sci. Technol. 36 (1992) 180.
[4] R. Srinivasan, J. Appl. Phys. 73 (1993) 2743.
[5] T. Zyung, H. Kim, J.C. Postlewaite, D.D. Dlott, J. Appl. Phys. 65 (1989) 4548.
[6] D.E. Hare, S.T. Rhea, D.D. Dlott, R.J. D'Amato, T.E. Lewis, J. Imag. Soc. Technol. 42 (1998) 90.
[7] C.R. Phipps (Ed.), High-power Laser Ablation, Vol. 3343, SPIE, Bellingham, WA, 1998.
[8] W.A. Tolbert, I.-Y.S. Lee, D.D. Dlott, M.M. Doxtader, E.W. Ellis, J. Imag. Sci. Technol. 37 (1993) 411.
[9] S.G. Koulikov, D.D. Dlott, Opt. Photonics News 11 (2000) 26.
[10] V.P. Veiko, S.M. Metev, A.I. Kaidanov, M.N. Libenson, E.B. Jakovlev, J. Phys. D 13 (1980) 1565.
[11] V.P. Veiko, S.M. Metev, K.V. Stamenov, H.A. Kalev, B.M. Jurkevitch, I.M. Karpman, J. Phys. D 13 (1980) 1571.
[12] D. Albagli, M. Dark, L.T. Perelman, C. von Rosenberg, I. Itzkan, M.S. Feld, Opt. Lett. 19 (1994) 1684.
[13] D. Albagli, M. Dark, C. von Rosenberg, L. Perelman, I. Itzkan, M.S. Feld, Med. Phys. 21 (1994) 1323.
[14] R. Srinivasan, Science 234 (1986) 559.
[15] I. Itzkan, D. Albagli, M.L. Dark, L.T. Perelman, C. von Rosenberg, M.S. Feld, Proc. Natl. Acad. Sci. USA 92 (1995) 1960.
[16] W.A. Tolbert, I.-Y.S. Lee, X. Wen, M.M. Doxtader, E.W. Ellis, D.D. Dlott, J. Imag. Sci. Technol. 37 (1993) 485.
[17] S.G. Koulikov, D.D. Dlott, J. Imag. Sci. Technol. 44 (2000) 111.
[18] D.E. Hare, J. Franken, D.D. Dlott, J. Appl. Phys. 77 (1995) 5950.
[19] J.-D. Kamminga, T.H. de Keijser, R. Delhez, E.J. Mittemeijer, J. Appl. Phys. 88 (2000) 6332.
[20] Y.B. Zel'dovich, Y.P. Raiser, Physics of Shock Waves and High-temperature Hydrodynamic Phenomena, Academic Press, New York, 1966.
[21] D.R. Lide (Ed.), Handbook of Chemistry and Physics, 81st Edition, CRC Press, Cleveland, OH, 1996.
[22] D.E. Hare, S.T. Rhea, D.D. Dlott, R.J. D'Amato, T.E. Lewis, J. Imag. Sci. Technol. 41 (1997) 291.
[23] G.A.J. Amaratunga, M.E. Welland, J. Appl. Phys. 68 (1990) 5140.
[24] D. Maydan, Bell Syst. Technol. J. 50 (1971) 1761.
[25] I.-Y.S. Lee, W.A. Tolbert, D.D. Dlott, M.M. Doxtader, D. Arnold, D. Foley, E.R. Ellis, J. Imag. Sci. Technol. 36 (1992) 180.
[26] D.E. Hare, S.T. Rhea, D.D. Dlott, J. Imag. Sci. Technol. 41 (1997) 588.
[27] Y.S. Touloukian, C.Y. Ho, Thermophysical Properties of Matter, The TPRC Data Series, IFI/Plenum, New York, 1970.
[28] R.J. Roark, W.C. Yound, Formulas for Stress and Strain, 5th Edition, McGraw-Hill, New York, 1975.